TU Delft

Delft University of Technology

Document Version
Final published version

Licence
CC BY

Citation (APA)
Wiegel, M., de Boer, W., van Koningsveld, M., van der Hout, A., & Reniers, A. (2021). Global mapping of seaport operability risk indicators using open-source metocean data. *Journal of Marine Science and Engineering*, *9*(7), Article 695. https://doi.org/10.3390/jmse9070695

Important note
To cite this publication, please use the final published version (if applicable).
Please check the document version above.

Copyright
In case the licence states “Dutch Copyright Act (Article 25fa)”, this publication was made available Green Open Access via the TU Delft Institutional Repository pursuant to Dutch Copyright Act (Article 25fa, the Taverne amendment). This provision does not affect copyright ownership.
Unless copyright is transferred by contract or statute, it remains with the copyright holder.

Sharing and reuse
Other than for strictly personal use, it is not permitted to download, forward or distribute the text or part of it, without the consent of the author(s) and/or copyright holder(s), unless the work is under an open content license such as Creative Commons.

Takedown policy
Please contact us and provide details if you believe this document breaches copyrights.
We will remove access to the work immediately and investigate your claim.

This work is downloaded from Delft University of Technology.

Journal of *Marine Science and Engineering*

MDPI

Article

Global Mapping of Seaport Operability Risk Indicators Using Open-Source Metocean Data

Matijs Wiegel [1,2,*], Wiebe de Boer [1,2], Mark van Koningsveld [1,3], Arne van der Hout [1,2] and Ad Reniers [1]

[1] Faculty of Civil Engineering and Geosciences, Delft University of Technology, P.O. Box 5048, 2600 GA Delft, The Netherlands; wiebe.deboer@deltares.nl (W.d.B.); m.vankoningsveld@tudelft.nl (M.v.K.); a.j.vanderhout@tudelft.nl (A.v.d.H.); a.j.h.m.reniers@tudelft.nl (A.R.)
[2] Department of Harbour Coastal & Offshore Engineering, Deltares, P.O. Box 177, 2600 MH Delft, The Netherlands
[3] Engineering and Estimating Department, Van Oord, P.O. Box 8574, 3009 AN Rotterdam, The Netherlands
* Correspondence: matijs.wiegel@gmail.com; Tel.: +31-610-51-93-51

Abstract: Seaport operability is key to the economic viability of ports. Metocean conditions (e.g., wind, short waves, and infragravity waves) affect this operability when certain thresholds are exceeded. This paper describes a method for the global mapping of seaport operability risk indicators using open-source metocean data. This global-scale assessment provides a geographic overview of operability risks and first-order insights into the most relevant metocean risk indicators at each location. The results show that locations around the equator and inland seas have lower operability risk than locations farther away from the equator. "Hotspots" are mainly located along the southern capes (Cape of Good Hope, Leeuwin, Horn), around the 'Roaring Forties', and at exposed locations along the oceans. Of the metocean parameters considered, short waves are found to be the most critical risk indicator for port operability at most locations. Using (the insights of) this study, port authorities, operators, and designers can prepare for metocean risks at an early stage and effectively respond with mitigation measures and layout adjustments to improve port operability.

Keywords: seaports; port operability; global mapping; downtime; metocean; wind; short waves; infragravity waves; ERA5

check for updates

Citation: Wiegel, M.; de Boer, W.; van Koningsveld, M.; van der Hout, A.; Reniers, A. Global Mapping of Seaport Operability Risk Indicators Using Open-Source Metocean Data. *J. Mar. Sci. Eng.* **2021**, *9*, 695. https://doi.org/10.3390/jmse9070695

Academic Editor: Mihalis Golias

Received: 5 May 2021
Accepted: 20 June 2021
Published: 24 June 2021

Publisher's Note: MDPI stays neutral with regard to jurisdictional claims in published maps and institutional affiliations.

Copyright: © 2021 by the authors. Licensee MDPI, Basel, Switzerland. This article is an open access article distributed under the terms and conditions of the Creative Commons Attribution (CC BY) license (https://creativecommons.org/licenses/by/4.0/).

1. Introduction

International shipping is key to the global economy and responsible for the transport of 80% of the world's trade by volume and over 70% of world's trade by value in 2018 [1]. Seaports are crucial nodes in the world's supply chains and play an important role in the development of regional and national economies [2]. The performance of ports, and related supply chains, is affected by weather related downtime, e.g., by wind and waves [3]. Accounting for these weather conditions in port design and operations is important to minimize port downtime, optimize port competitiveness, and ensure the continuity of supply chains.

We define 'port operability' as the degree to which safe and reliable port operations (e.g., navigation, tugging, mooring, berthing, on/offloading) can be guaranteed. It is determined, among others, by environmental conditions, dynamic ship response, port infrastructure design (e.g., layout, fenders, handling means), and human factors (for an overview, see [4]). Here, we focus on port operability risks related to metocean conditions in terms of wind and waves.

Increasing vessel dimensions cause wind to become a more critical factor in port operations, both for maneuvering and mooring. Large sea waves can hinder the tugboats and influence the roll motions of the ship. Moored vessels may be sensitive to infragravity (IG) waves, when long wavelengths and wave periods are close to the vessel's natural response periods (eigen periods) [5–7]. In addition, preventing such IG waves from

penetrating into the port basins can be difficult due to their large wavelengths [8–11]. Careful site selection and infrastructure design can help to minimize port downtime due to these conditions, e.g., by natural sheltering, man-made protective structures, or other mitigating measures. However, it is difficult and expensive to prevent downtime entirely.

Information on the local wind and wave conditions is essential to assess port operability risks and for the design of appropriate protection structures or the dimensioning of other mitigating measures. Usually, extreme conditions are used for the structural design of port infrastructure, whereas regular (annual average) conditions are used to assess the port's operability. To estimate local nearshore wave conditions, typically, offshore wave data are transformed to the nearshore via numerical models, such as SWAN (Simulating Waves Nearshore) [12], STWAVE (Steady-State Spectral Wave Model) [13] or MIKE 21 SW [14]. Other models can be used to assess the wave penetration into the port. For example, PHAROS (Program for Harbour Oscillations, a mild-slope model) [15], TRITON (a Boussinesq-type wave model) [16], and SWASH (Simulating WAves till SHore, a non-hydrostatic wave-flow model) [17]. The (wave) conditions inside the port are used to predict vessel motions at the berth and compare these against operability thresholds.

Operability thresholds typically depend on the conditions under which the mooring systems and cargo handling equipment can operate safely (see [4]). The likelihood that wind and wave conditions exceed predefined operability thresholds at a given location is an indicator of the weather-related downtime risk that a seaport at this location can be subject to. Despite the definition of objective thresholds, the decision to actually stop port operations is subjective and made by the operators [4].

Several studies have been conducted to estimate the wave conditions in a port at national or local scale [18–21]. Most of these studies focus on a single operability indicator, e.g., either short waves [18,19] or infra-gravity waves [20,21]. Recent studies also focus on the effects of climate change on port operability [4,22–24], mostly focusing on indicators such as overtopping [25,26], wave agitation [27], sea level rise (SLR) [28], or a combination of wave agitation and SLR [29]. However, due to the local focus of these studies, they do not allow for an intercomparison of the operability of port locations.

Rather than focusing on threshold-based decision making tools for operators of individual ports [4,22,23], the growing availability and extent of global reanalysis databases with atmospheric and ocean parameters [30] has enabled large-scale studies on ports, e.g., at continental scale [31] or even at global scale [24,32]. Often, these studies focus on existing ports only, which make them less suitable to analyze potential new port locations in terms of operability indicators. A global-scale assessment, including non-port locations, of port operability risk indicators as well as their relative importance is currently lacking.

This paper presents a novel method for the global mapping of seaport operability risk indicators for both existing and potentially new port locations. By analyzing 40 years of open-source metocean data on wind, short wave, and IG wave conditions at an hourly interval, we provide first-order (viz. pre-intervention) insights into which metocean parameters contribute most to seaport operability risks along the world's coastlines. This offers the opportunity to gain global-scale insights into spatial and temporal variations in port operability risk. Furthermore, we show how variations in winds and waves (e.g., due to climate change) are likely to affect port suitability around the world. Using the insights of this study, the seaport sector can (better) prepare for metocean risks at an early stage, account for them in site selection, and effectively respond with mitigation measures and layout adjustment to improve port operability.

2. Method for Global Mapping of Seaport Operability Risks Based on Metocean Data

To assess and map the operability risk related to wind, short wave and IG wave conditions at a global scale, we make use of a dataset that has global coverage yet sufficient detail. There are multiple global metocean databases available, ranging from actual observations from wave buoys and tidal gauges to reanalysis hindcast datasets which combine model data with satellite observations. For this paper, the global atmospheric European Centre

for Medium-range Weather Forecasting Re-Analysis 5th (ERA5) generation dataset [33] is used.

Currently, the ERA5 dataset has the highest resolution in time and space and is sufficiently long to estimate the average port operability risk over a larger period. The ERA5 data are open source and retrieved from the Copernicus Climate Change Service Climate Data Store (CDS) https://cds.climate.copernicus.eu/ (accessed on 1 November 2019). The ERA5 dataset contains wind speeds and spectral wave data on a regular grid with a spatial resolution of 0.5° × 0.5° at an hourly time interval. Although the database is continuously updated with new data, this study makes use of the data from 1 January 1979 to 31 December 2018. The following 4 steps are executed to quantify and map port operability risk at a global scale:

1. Retrieve the relevant metocean conditions from the ERA5 database (see Section 2.1).
2. Estimate and analyze port operability risk (see Section 2.2).
3. Validate the approach with existing port locations (see Section 2.3).
4. Expand the validated approach to a global grid (see Section 2.4).

2.1. Retrieve the Relevant Metocean Conditions from ERA5

2.1.1. Wind

The ERA5 database [33] contains the wind speeds at a height of 10 m above the Earth's surface in meters per second. U_{10} is the Eastward component (i.e., the horizontal speed of air moving towards the east) and V_{10} is the Northward component. For each coastline coordinate (obtained from the Natural Earth Data [34] coastline shapefile), the nearest ERA5 grid point is selected to retrieve the metocean data. The ERA5 grid points are selected at least 0.1° and not farther than 0.8° (respectively 10–100 km) away from the coastline coordinates. In this way it is ensured that the ERA5 information is sufficiently far away not to be influenced by small-scale geomorphological features such as islands, flats, ridges or troughs (which are not well captured in the ERA5 resolution), yet sufficiently close to the coast to have representative conditions. The U_{10} and V_{10} are retrieved from the ERA5 database and combined into the horizontal wind speed according to Equation (1):

$$\text{wind speed } = \sqrt{U_{10}^2 + V_{10}^2}, \quad (1)$$

It is assumed that the offshore wind climate is representative for the port location. This is likely to be a conservative estimate, as possible wind speed reductions due to the presence of land mass or infrastructures are not accounted for. The wind related port operability risk is therefore a conservative estimate (i.e., probably the actual wind related operability is a bit higher than our estimate).

2.1.2. Short Waves

In terms of short waves, the following wave characteristics are retrieved from the ERA5 database [33]: significant height of combined wind waves and swell (m), mean wave direction (°), mean wave period (s) and the offshore water depth (m). Because the wave conditions are obtained from ERA5 grid points offshore (see Section 2.1.1), the wave conditions may come from multiple directions (including from land). Only the short waves with a direction towards the port/coast are interesting for the port operability assessment. Therefore, short waves propagating seawards are removed from the short-wave analysis. This is done by calculating the angle between the ERA5 grid point and the closest coastline location with respect to North. Only those wave conditions are included that have a mean wave direction of ±90° of the angle between those points.

Normally, a port operability assessment is based on the nearshore mean wave conditions. However, since the ERA5 wave dataset has a spatial resolution of 0.5° × 0.5° and grid points are selected at least 0.1° off the coast, the retrieved ERA5 data can be 10–55 km offshore. Therefore, local operability assessments typically transform offshore wave conditions to the nearshore by means of numerical models with detailed local bathymetries and

(detailed) wave physics. Given the global scale of the assessment in this paper, carrying out such detailed assessments for every coastal region is not considered feasible in terms of the required data handling and computational effort. To overcome this hurdle, we make use of a simplified approach that relies on a wave energy balance [35].

Due to the absence of reliable nearshore bathymetric data on a global scale, we assumed an alongshore uniform coast with parallel depth contours and a gradually linear depth profile. The nearshore waves are derived at water depth of 20 m, which is comparable with drafts of the largest vessel sizes (more than 20,000 TEU container ships) and the port depths of the largest seaports. Detailed nearshore processes that are influenced by port layout and infrastructure, such as wave reflections and diffraction, are neglected. This assumption is considered defendable, since in this paper we focus on port operability risk at a pre-intervention level.

To estimate nearshore wave conditions, the following processes in which the wave characteristics are affected by the seabed are included: change of the direction of the waves (refraction) and wave height (shoaling) and finally breaking [35]. To calculate the effect of refraction on nearshore wave height, the shoreline orientation (°) is estimated from a coastline shapefile obtained from Natural Earth Data [34] consisting of 342,070 coordinates to draw the coastlines. For each ERA5 grid point that is considered in the analysis, the closest coordinate on the coastline shapefile is found. Left and right from this coastline point, the 4 closest coordinates of the coastline shapefile are averaged. Via the averaged coordinates left and right, the coastline orientation is calculated, which is then converted to the normal of the coastline. To test the accuracy of this method, 10 random sample locations have been checked manually, in addition to complex geometries (e.g., estuaries, inland seas, inlets, islands) and shoreline orientation estimation. Based on the outcome of these checks, we found this automatic shoreline orientation method to be sufficiently reliable for the purpose of this study.

2.1.3. Infragravity Waves

To provide an estimate of the infragravity (IG) wave conditions with a frequency of 0.004–0.04 Hz (25 s–250 s) that could be expected in the port, the incoming bound (forced) IG wave conditions are estimated at a nearshore water depth of 20 m based on the nearshore (spectral) wave climate. The same retrieval method as in Section 2.1.2 is applied, but this time including all wave directions, also from land. As IG waves go around defense structures like breakwaters, all wave directions are considered. IG wave height is determined for relevant combinations of the nearshore significant wave height (m) and the peak period (s). The IG waves are estimated by the widely accepted theory of Herbers et al. [36], who stated that second-order non-linear theory from Hasselmann [37] accurately predicts locally forced infragravity motions. From the estimated bound waves, the representative wave height $H_{m0,Low}$ and mean wave period $T_{m01,Low}$ are determined based on the zeroth-order and first-order moments of the spectral density. The equivalent expression described by Van Dongeren et al. [38] is used and can be found in Appendix A. Estimating the infragravity wave height for all (hourly) input values is computationally intensive. To tackle this problem, a look-up table is developed for 250 × 250 combinations of the nearshore significant wave height and peak period with a step size of 0.05 m and 0.1 s ranging from 0–12.50 m and 0–25 s, covering all common operational wave conditions with a nearshore water depth of 20 m. This method has only small inaccuracies due to the fact that it rounds the input parameters to the nearest value on the axes of the look-up table, but then interpolates them. This approach makes it possible to estimate the IG wave heights on a global scale at an hourly time interval.

2.2. Estimate and Analyze Port Operability Risk Using a Conditioned Thresholding Approach

To assess port operability risks, we make use of the conditioned thresholding approach from Molina-Sanchez et al. [4]. This approach enables us to estimate the overall operability by evaluating multiple operability risk indicators at the same time. Each operability

risk indicator (i.e., wind, short waves, and IG waves) is analyzed based on a mono-parametric thresholding approach. This approach links the vessel oscillations to a single metocean parameter with a fixed threshold [4]. When the metocean indicator value is below its threshold, the risk of impact on port operability is considered 'low'; when the value is above the threshold, the risk of impact on port operability is considered 'high'. The fixed thresholds are derived from literature, viz. guidelines from PIANC (Permanent International Association for Navigation Congresses) [39–41], international guidelines [42,43], and handbooks [44,45], and are primarily meant to illustrate the method and provide preliminary estimates of maximum allowable metocean conditions, shown in Table 1.

Table 1. Operability thresholds based on literature.

Metocean Indicator	Operability Threshold	Literature References
Wind speed [m/s]	13.8	Container terminals will significantly reduce their operability for wind speeds higher than the Beaufort scale 6 (13.8 m/s) [1].
Short wave height [m]	2.0	Tugboats remain navigable with a short-wave height not higher than 1.5–3.0 m to attach tugs to a ship [2].
IG wave height [m]	0.05	Based on an empirical relation [3] and international guidelines [4].

[1] [39,42,44]; [2] [41]; [3] [43]; [4] [40].

The conditioned thresholding approach computes the amount of time each metocean indicator stays below its threshold as well as the interval between, the frequency of, and the duration of exceedance events (visualized in an illustrative plot in Figure 1). For the analysis of a single indicator, the following five definitions are used:

1. Availability: The duration that a metocean indicator is below its threshold (% per year).
2. Interval: The average time between threshold exceedance events (time interval between events).
3. Conditional availability: The duration that a metocean indicator is below its threshold without short intervals of less than or equal to 4 h (% per year).
4. Frequency: The average number of operability threshold exceedance events (events per year).
5. Duration: The average time of exceedance events (time duration in hours per event).

We define the term "availability", for each individual metocean indicator (P_{wind}, P_{waves} and $P_{IGwaves}$) as the percentage of time that the metocean indicator is below its threshold. Values above the operability threshold are classified as 'unavailable'. The threshold-based approach is complemented by evaluating the "interval" between exceedance events (i.e., the time between a down-crossing and subsequent up-crossing as shown in Figure 1) following Campos et al. [22]. It is expected that port operators will not resume their operations when there is a high probability that the threshold will be exceeded again on short term. Therefore, it is assumed that short intervals less than or equal to 4 h (purple lines in Figure 1) are classified as 'unavailable'. Hence, a long period of multiple short interval exceedances is treated as one exceedance event. The remaining non-exceedance events are called "conditional availability" (green line in Figure 1).

The "frequency" and "duration" are used to analyze port operability risk in more detail. By analyzing the frequency, insights are generated regarding the number of times port operations potentially need to shut down and restart again, which limits the uptime. The average time of exceedance events per year ("duration") gives insights into how long a period of potential unavailability last. This allows for differentiation between ports with potentially short and long periods of downtime. Short periods of downtime could be compensated for more quickly than longer periods of downtime.

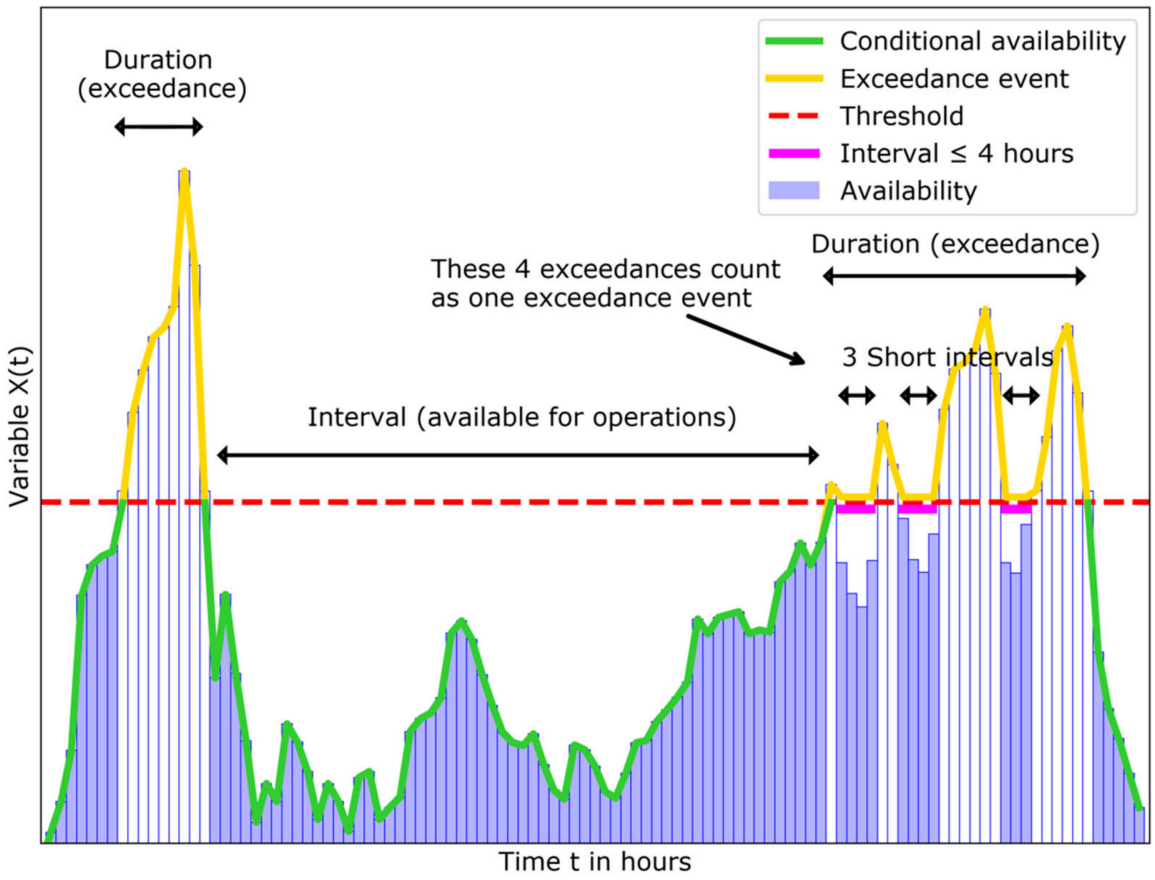


Figure 1. Illustration of the definitions to estimate and analyze the port operability risk via the conditional availability, exceedance interval, frequency and duration.

By combining the conditional availability for each individual metocean indicator (P_{wind}, P_{waves} and $P_{IGwaves}$, dotted lines in Figure 2), we define the overall conditional availability (P_{total}). P_{total} is defined as the percentage of time that all metocean indicators are below their thresholds, excluding short intervals of less than or equal to 4 h. It is assumed that the port will be operational without loss of production during that time. This approach allows us to compare different locations and define main drivers of these risks, and it may also be helpful to assess the sensitivity to changing metocean indicators.

The conditioned thresholding approach is simplistic, because it assumes that operability can be estimated from an aggregated metocean indicator only, without accounting for the characteristics of the ship, mooring system, and port layout. Nevertheless, it is effective to distinguish the port operability risk indicators which are seen as a good indicator of whether and which metocean parameters play a role in the operability of a port. An unfortunate combination of the individual indicators (even when below their individual thresholds) may cause downtime due to excessive ship motions [4]. Nevertheless, the conditioned thresholding approach is considered appropriate for first-order operability risk estimates for this global-scale assessment.

NB: in the remainder of this paper, we use the term high port operability risk (i.e., high risk of downtime) if the conditional availability (P_{total}) is low and, conversely, low port operability risk if P_{total} is high. The following port operability risk levels are used: $P_{total} > 95\%$ (low), $85\% < P_{total} \leq 95\%$ (medium), $75\% < P_{total} \leq 85\%$ (high) and $P_{total} \leq 75\%$ (very high).

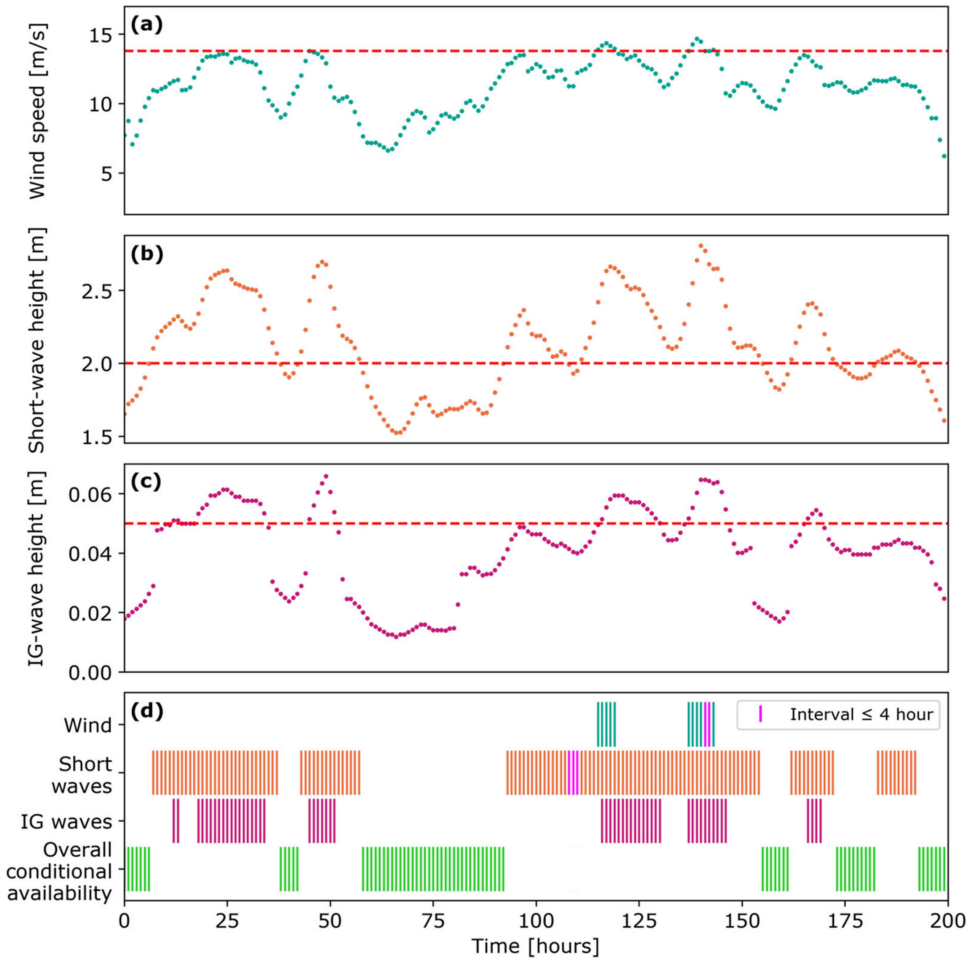


Figure 2. Schematic representation of the conditioned thresholding approach. The upper three panels show snapshots of the time series of the metocean indicators: (**a**) wind speed; (**b**) short wave height; and (**c**) IG wave height. The red-dashed lines represent the thresholds for each indicator. The lower panel (**d**) shows the resulting conditional unavailability for each indicator (cyan for wind, orange for short waves, purple for IG waves) and the overall remaining availability (P_{total}, in green).

2.3. Validate the Approach with Existing Port Locations

To validate whether the port operability risk that is derived from global datasets is sufficiently meaningful for individual port locations, we applied the method to 10 port locations, 5 of which are known for either having 'serious operability issues' and another 5 known to have 'limited operability issues'. Ideally, we would have compared our estimates with actual port operability or downtime data from port operators to validate our global estimates. However, due to confidentiality, this information is often not publicly available. Instead, for the selection of ports with known 'serious operability issues', we referred to literature. Several authors have published papers on ports with known operability issues related to wind and in particular short waves and IG waves:

- Long Beach (USA) [46]
- Tomakomai (Japan) [47]
- Salalah (Oman) [48]
- Cape Town (South Africa) [49]
- Geraldton (Australia) [50,51]

For ports with 'limited operability issues', we selected ports with open layouts (i.e., environmentally exposed without protection structures or other mitigating measures) using

Google Maps [52] under the assumption that such open layouts were feasible because of a mild wave climate:

- Doraleh (Djibouti)
- Jeddah (Saudi Arabia)
- Hay Point (Australia)
- Shanghai (China)
- Hadera (Israel)

After analyzing these 10 port locations they are classified in a confusion matrix (see Figure 3) to check the goodness of fit of the port operability risk estimate via a true or false positive (or negative) compared to our above classification.

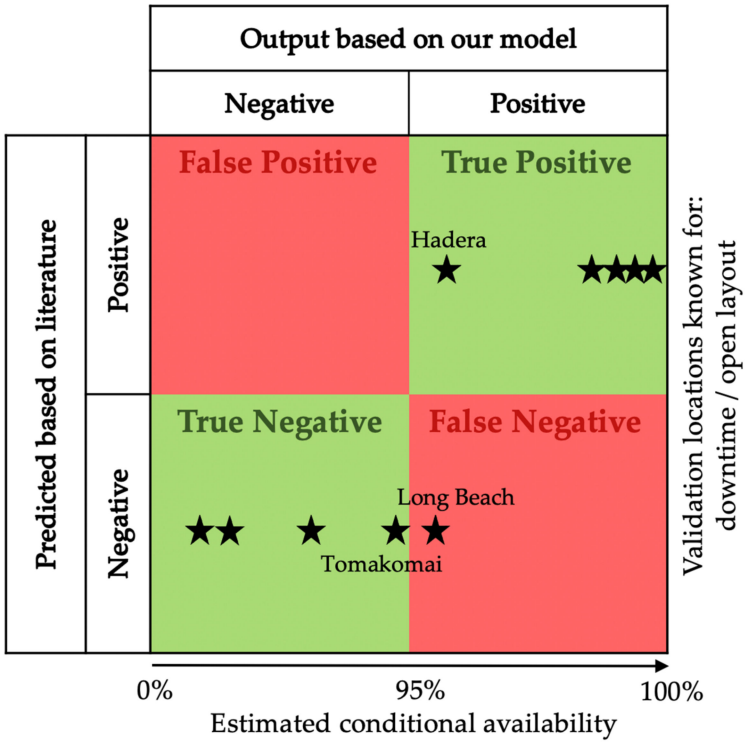


Figure 3. Confusion matrix classification: True or False Positive (or Negative). A True Positive (TP) is an outcome where the model correctly predicts the positive class. Similarly, a True Negative (TN) is an outcome where the model correctly predicts the negative class. A False Positive (FP) is an outcome where the model incorrectly predicts the positive class. And a False Negative (FN) is an outcome where the model incorrectly predicts the negative class. The stars correspond to the 10 (existing) port locations.

To compare the operability risk indicator with literature, we need a reference value to determine whether a location has low or high operability risk. In this paper, the 95th percentile (p_{95}) is used as a theoretical threshold. This 95th percentile is chosen based on international standards and recommendations [40,44]. When the combined metocean indicators are below their operational threshold for 95% of the time (i.e., overall conditional availability of 95%), it is an indication that a (port) location has low operability risk. This user defined 95th percentile threshold may be adjusted for other study purposes, because different cargo types require different availability limits at the berth. For oil and gas terminals, availability is typically accepted to be lower, e.g., 90% berth availability per year, and for container terminals it will often be slightly higher, with 98% availability [44]. The 95% threshold is mainly chosen here to illustrate the possibilities on how to quantify and classify the outcomes.

The overall conditional availability is visualized in Figure 4 and outlined in Table 2. Four out of five port locations known for an open layout have an extremely high overall

conditional availability ≥99.4% (see Figure 4 and Table 2), indicating very mild metocean conditions in general. The Port of Hadera has an overall conditional availability estimate of 96.2%, which is a small outlier but still exceeds the chosen limit (95%). Looking at Figure 4, this is mainly due to short waves. The offshore deep-water terminal in front of the coast of Hadera handles liquid and dry bulk cargo, while the other four port locations handle all kinds of cargo, including containers, which are subject to more stringent conditions. The short-wave height limits for tankers and dry bulk vessels may exceed the chosen 2.0 m short-wave height limit [44]. The estimate of the overall conditional availability for the Port of Hadera is therefore indicated as conservative. Therefore, it must be concluded that our approach does not reflect such details for ports with less stringent conditions (i.e., liquid and dry bulk terminals), although by selecting a different threshold for P_{total}, the analysis can be tuned for specific study objectives.

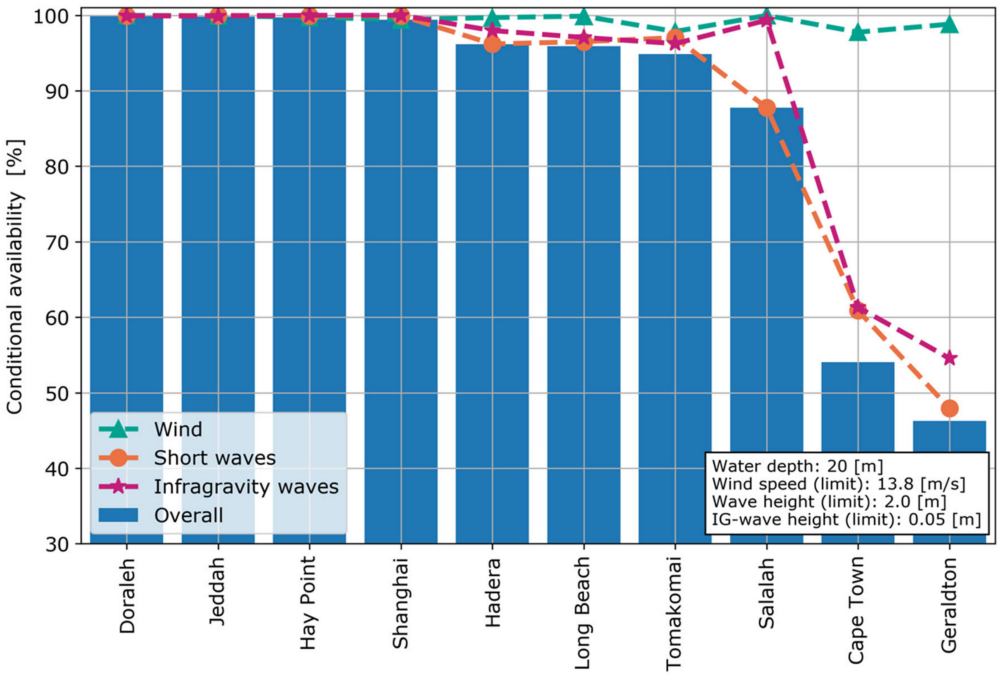


Figure 4. The overall conditional availability for 10 (existing) port locations including drivers (dotted lines). The left 5 ports have an open layout and the right 5 are known for operability issues. Input/thresholds used in the methodology are given in the lower right corner.

Table 2. Outcomes of the validation study for 10 (existing) port locations. The top 5 ports have an open layout and the bottom 5 are known for operability issues.

Port	Overall Conditional Availability [%]	Conditional Availability per Risk Indicators			Frequency [Events/year]	Average Duration per Event [hours]	Mean Wave Period [s] [1]
		Wind [%]	Short Waves [%]	IG Waves [%]			
Doraleh	99.9	99.9	99.9	99.9	1.5	8.6	4.3
Jeddah	99.8	99.9	99.9	99.9	1.4	9.8	4.5
Hay Point	99.7	99.7	99.9	99.9	2.2	10.9	3.4
Shanghai	99.4	99.4	99.9	99.9	5.4	9.5	3.2
Hadera	96.2	99.7	96.2	98.0	12.5	27.1	5.1
Long Beach	95.9	99.9	96.5	97.1	16.5	21.9	9.7
Tomakomai	94.9	97.8	97.0	96.2	31.8	14.1	6.6
Salalah	87.8	99.9	87.8	99.3	17.9	60.0	7.4
Cape Town	54.1	97.8	60.9	61.3	81.3	49.5	9.5
Geraldton	46.2	98.8	47.9	54.6	86.6	54.4	10.1

[1] The mean wave period is added to show the difference in type of climate between the 5 open layout locations and the 5 locations known for their downtime.

Figure 4 presents the conditional availability values for the individual port operability risk indicators (dotted lines), next to the overall conditional availability (blue bars). If an individual indicator value is close to the blue-colored bar, it means that this driver or port operability risk indicator is exceeded during almost all exceedance events for a given location, and thereby likely to be the most dominant driver. When all individual drivers are close together, it is an indication of strong interdependence of those drivers. When this is not the case, and there is a difference between the lowest port operability risk indicator and the blue-colored bar (e.g., at the Port of Cape Town or Geraldton), it indicates that this individual port operability risk indicator does not exceed the threshold simultaneously with the other indicators and therefore occurs independently. In the examples of Cape Town and Geraldton, it is illustrated that threshold exceedance is strongly related to short and IG waves, independently of limiting wind conditions.

The frequency and duration of exceedance events also show a clear relative difference between the locations with an open layout and those known for downtime (see Table 2). The frequency has an order of magnitude difference (from 1.4 to 86.6 events/year). The average duration of an exceedance event has also an order of magnitude difference (from 8.6 to 60 h). The duration reveals that if a threshold(s) is exceeded, the port is unavailable for at least 8 h. The frequencies of the Port of Salalah are significantly lower than the average for ports known for their downtime, but the average duration of an exceedance event is the highest of all. This can be explained by the monsoon season, which is active for only a couple of months a year, but the weather conditions are much more extreme than the average conditions during that period. Another difference can be observed when looking at the mean wave period in Table 2. The 5 open layout locations (first 5 locations in Table 2) have a mean wave period of 3–5 s, which is indicative for a wind wave climate, the 5 locations known for their downtime have a mean wave period of 7–10 s, which is more indicative for a swell wave climate. So, in addition to the overall conditional availability, this shows that there are more differences between locations with an open layout and locations known for their downtime, which can provide interesting insights. It was expected that downtime associated with short waves and IG waves would be the main driver for the selected ports with known operational issues, as the selected validation ports were known for this.

After analyzing the overall conditional availability, the 3 individual metocean indicators are considered (see Table 2). For all 10 (existing) port locations the overall conditional availability for wind is not exceeded, i.e., for at least 95% of the time all the 10 port locations are available for port operations in terms of wind. In terms of short waves, 3 out of 5 locations known for operability issues are well below the 95th percentile. There is also a clear distinction for the IG waves, 4 out of 5 locations known for downtime are close to or well below the 95th percentile. The port of Salalah is a slight outlier. Literature suggests that this port suffers from IG waves [48], but our approach estimates a 99.3% conditional availability for IG waves, which is well above the 95th percentile, making short waves the dominant metocean driver. This can perhaps be explained by resonance effects due to layout of the port that may play a role but is not included in our global approach. Other possible explanations could be that the monsoon conditions, which generally lead to unavailability, are not well represented in the global metocean dataset [53], and during tropical cyclones the significant wave height is underestimated [54].

For 9 out of 10 cases, our approach is able to correctly predict the presence/absence of port operability issues when using the 95th percentile of overall conditional availability as separation point (visualized in a confusion matrix in Figure 3). The port of Long Beach is a misclassification with an overall conditional availability of 95.9% which is higher than expected from literature [46]. The port of Long Beach is sheltered by a large offshore island, which can have effects on the wave propagation (e.g., sheltering, reflection and diffraction) which is not included in our approach. This can be the cause of the underestimation of the wave height. Therefore, it must be concluded that our approach does not always provide reliable operability estimates in locations with islands or other

(large-scale) geomorphological features offshore or in the nearshore. However, overall, it can be concluded that our approach is able to make reliable first-order estimates of port operability risk due to wind, short waves, and IG waves.

2.4. Expand the Validated Approach to a Global Grid

To create a global grid along the world's coastline, a shapefile from Natural Earth Data [34] with a 10 million-scale raster data was used as the reference coastline, consisting of 342,070 coordinates. For each coastline location, the nearest ERA5 grid point is selected under the same conditions and for the same reason as already explained in Section 2.1, at least 0.1° and not farther than 0.8° away from the coastline coordinates. Hereafter, the duplicate ERA5 grid points were removed. This resulted in 4560 unique geographical locations along the world's coastline that could be used in our global analysis. Lastly, some manual adjustments have been made by removing grid points on the open ocean around small islands and within large estuaries due to the assumed large uncertainties from the ERA5 datasets in those areas.

3. Results

3.1. Global Spatial Patterns in Port Operability Risk

We classified and mapped 4560 locations along the world's coastline into operability risk levels based on their overall conditional availability (P_{total}) (see Figure 5). The following port operability risk levels are used: $P_{total} > 95\%$ (low), $85\% < P_{total} \leq 95\%$ (medium), $75\% < P_{total} \leq 85\%$ (high) and $P_{total} \leq 75\%$ (very high). Note that the locations that are classified as having a very high operability risk level (i.e., the hotspots) based on our method do not necessarily have to experience downtime in practice as factors such as port capacity, possible wave sheltering, and mitigating measures (e.g., breakwaters) have not been considered in the analysis. The classification merely provides a first estimate of where severe and where milder conditions can be expected.

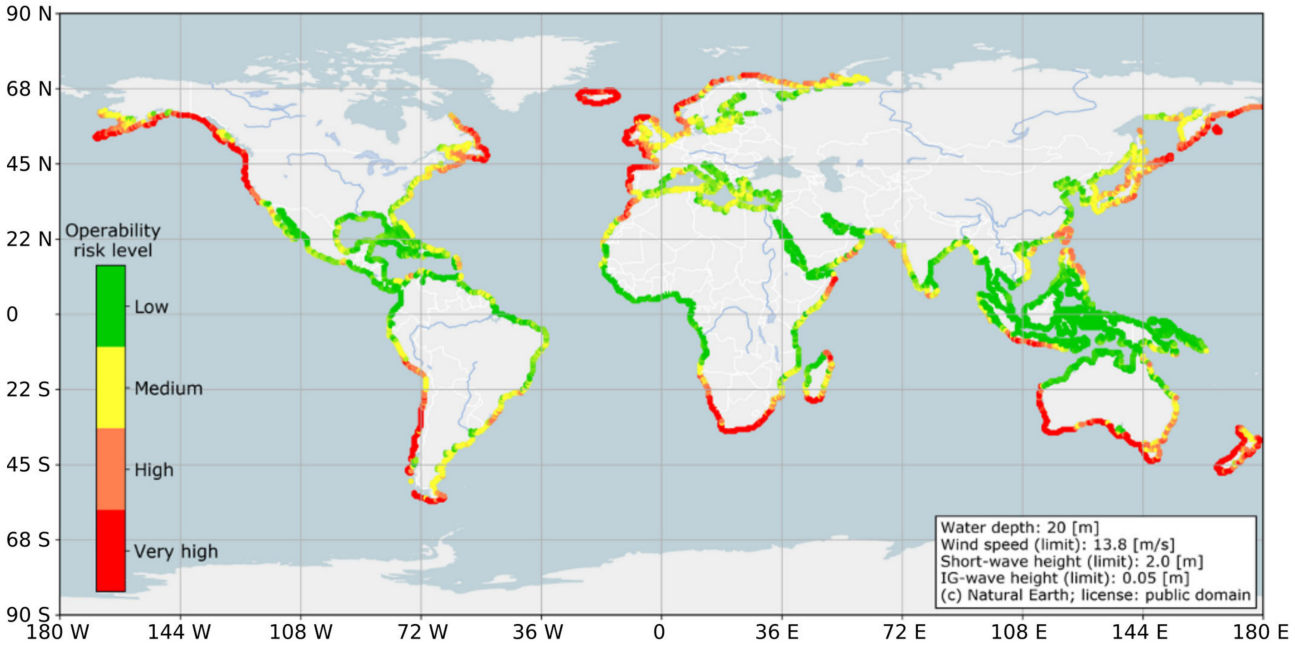


Figure 5. Geographical overview of port operability risk levels. Input/thresholds used in the method are given in the lower right corner.

The port operability risk levels vary considerably geographically, see Figure 5. The "hotspots" in terms of operability risk (indicated by the red dots in Figure 5) are mainly located along the southern capes (i.e., Cape of Good Hope, Leeuwin, Horn), around the 'Roaring Forties' (i.e., the region with frequently strong westerly winds between the

latitudes 40 and 50 degrees south of the equator), and at exposed locations along the oceans. Locations on and around the equator tend to have a lower operability risk (indicated by the green dots in Figure 5) than locations farther away from the equator (more orange and red dots in Figure 5). Around inland seas (such as the Red Sea and the Mediterranean), there is often a lower operability risk, which is probably related to a reduced exposure to the swell waves. Of the 4560 locations, 2336 (51.2%) have a low operability risk, 1048 (23%) medium, 491 (10.8%) high, and 685 (15%) very high (see Table 3). Our analysis indicates that, for almost half of the locations (classified as medium, high, or very high), mitigating measures may be required to guarantee a sufficient port operability level.

Table 3. Overview of the conditional availability of the 4560 locations, differentiated into risk indicators and event frequencies and duration and categorized in operability risk level classes.

Operability Risk Levels [%]	Locations [#]	Average Conditional Availability [%]	Conditional Availability per Risk Indicators			Frequency [Events/year]	Average Duration per Event [hours]
			Wind [%]	Short Waves [%]	IG Waves [%]		
Low	2336 (51.2%)	98.7	99.7	99.1	99.2	7.2	13
Medium	1048 (23%)	90.7	97.7	93.2	93.8	35.1	25
High	491 (10.8%)	80.6	95.7	85.4	85.5	54.5	35.7
Very high	685 (15%)	58.3	93.6	64.8	66.7	69.0	55
Total/Avg.	4560 (100%)	88.9	97.9	91.1	91.6	28	24.5

Our approach also allows us to analyze which metocean indicators are the most critical for the port operability (see Table 3). For all operability risk levels, the short waves are the most critical indicator, as short waves result in the lowest overall conditional availability for all operability classes. IG waves, which are derived from the short waves in our approach, result in slightly higher overall conditional availability percentages. Wind conditions are less important compared to the other metocean indicators. This result indicates that, for most locations, especially (the dampening of) short waves need to be considered in port design and operations.

Furthermore, we can quantify the frequency and duration of threshold exceedance events for each risk level. The frequency of exceedance events (number of events per year) increases rapidly with increasing operability risk levels (from 7.2 for low operability risk level to 69 for very high, see Table 3). The same applies to the duration of an exceedance event, which increases from 13 h on average for low operability risk level to 55 h for the very high level (see Table 3). An increase in frequency and duration could further hamper port operations, due to delays during shut down and restart procedures and the inability to make up for unavailable operation periods.

Insight into the main port operability risk drivers may allow port authorities, operators, and designers to identify and mitigate risks at an early stage. The main operability driver for a certain location is defined as that metocean indicator that has the lowest conditional availability value. Figure 6 shows the spatial distribution of the main operability drivers on a global map. Due to the correlation between short waves as input for the IG waves estimation, an additional 'Short & IG waves' class is added for a situation where these drivers are both dominant. This is assumed to be the case if their conditional operability values differ less than 1%. It must be noted that the map in Figure 6 does not indicate the port operability risk level of a location but only the main driver. So, Figure 6 shows which driver is most likely to affect the port operations, even though the port operability risk may be low for a certain location, as shown in Figure 5. Along the Pacific Ocean coastline, our approach shows that IG waves are the (potential) main driver for operability issues. Along the Atlantic Ocean coastline, a combination of multiple drivers is important, except for the east coast of South America, where short waves are the dominant driver. For the coastline along the Indian Ocean short waves are also the main driver. Around inland

seas and mainly Indonesia, locations can be observed where the wind acts as the main operability driver.

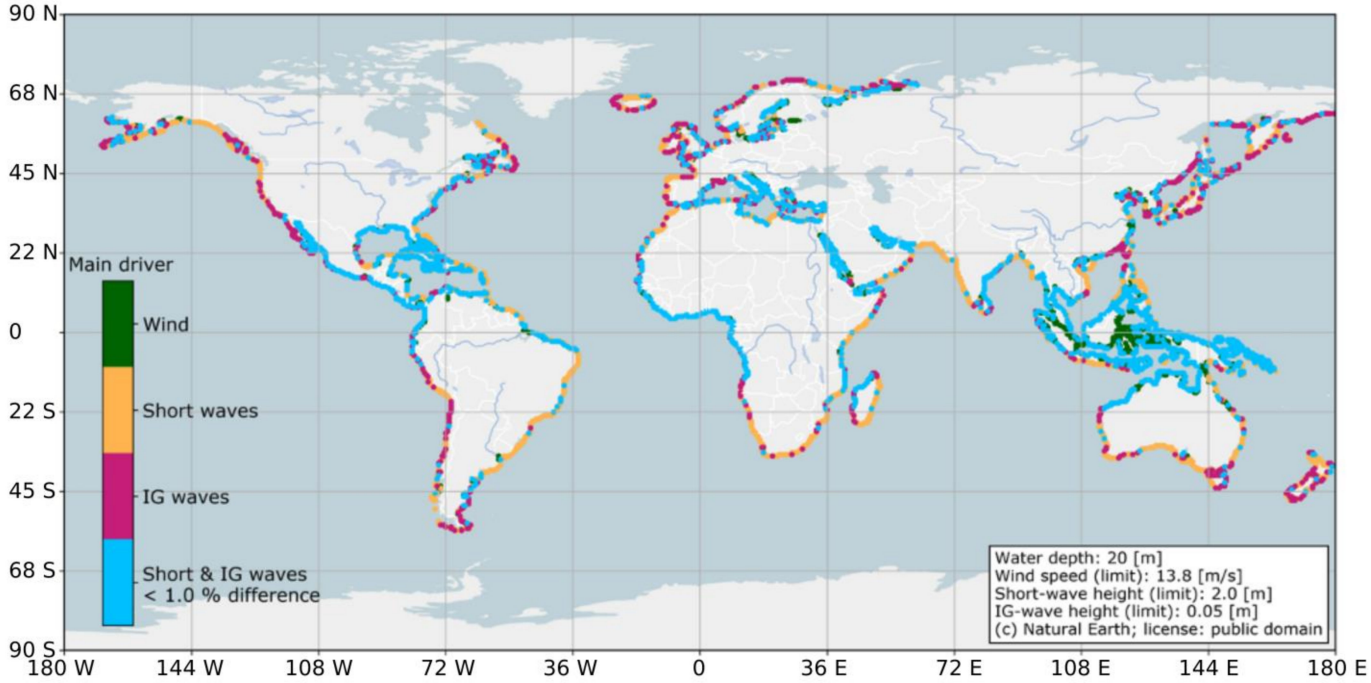


Figure 6. Geographical overview on the main drivers for port operability risks. Input/thresholds used in the method are given in the lower right corner.

The main drivers are short waves and IG waves (see Table 4). Often, these conditions coincide. Out of the 4560 locations, 1792 (39.3%) locations have a combination of Short & IG waves as their main driver, followed by short waves for 1433 (31.4%) locations. The number of locations with IG waves as main driver is 897 (19.7%) and 438 (9.6%) have wind as their main driver. Table 4 shows that wind, in contrast to the overall average conditional availability from Table 3, does have a significant impact for the lowest operability risk level: 421 (18% of the risk level) locations that are classified as low risk have wind as their main driver. Hence, when wind conditions are changing (for example due to climate change), these locations may still be susceptible to operability risks.

Table 4. Overview of the main operability-issues drivers for 4560 locations, differentiated into four operability risk indicator classes and categorized in operability risk level classes.

Operability Risk Levels [%]	Locations [#]	Main Drivers			
		Wind [#]	Short Waves [#]	Short & IG Waves [#]	IG Waves [#]
Low	2336 (51.2%)	421 (18.0%)	271 (11.6%)	1503 (64.3%)	141 (6.0%)
Medium	1048 (23%)	14 (1.3%)	493 (47.0%)	215 (20.5%)	326 (31.1%)
High	491 (10.8%)	2 (0.4%)	251 (51.1%)	43 (8.8%)	195 (39.7%)
Very high	685 (15%)	1 (0.1%)	418 (61.0%)	31 (4.5%)	235 (34.3%)
Total	4560 (100%)	438 (9.6%)	1433 (31.4%)	1792 (39.3%)	897 (9.7%)

3.2. Global Temporal Patterns in Port Operability Risk

3.2.1. Intra-Annual Trends

The effects of the intra-annual time scale on port operability risks are studied via the seasonality. To this end, the time series are divided into four separate seasons: boreal winter: December, January, and February (DJF); spring: March, April, and May (MAM); summer: June, July, and August (JJA); and autumn: September, October, and November (SON). The

different seasons are classified and mapped into operability risk levels in Figure 7. In the northern hemisphere, there is a clear difference between winter (DJF) with high operability risk and summer (JJA) with low operability risk. It is also clearly visible that during JJA there is a high operability risk around the coastline of the Arabian sea and Bay of Bengal. This can be explained by the Indian monsoon period and starting to be strong in JJA with increasing swell wave heights. The southern hemisphere shows a high operability risk year-round. This is probably related to the swell wave climate resulting from long fetches and year-round relatively higher wind speeds in the southern hemisphere than in the northern hemisphere.

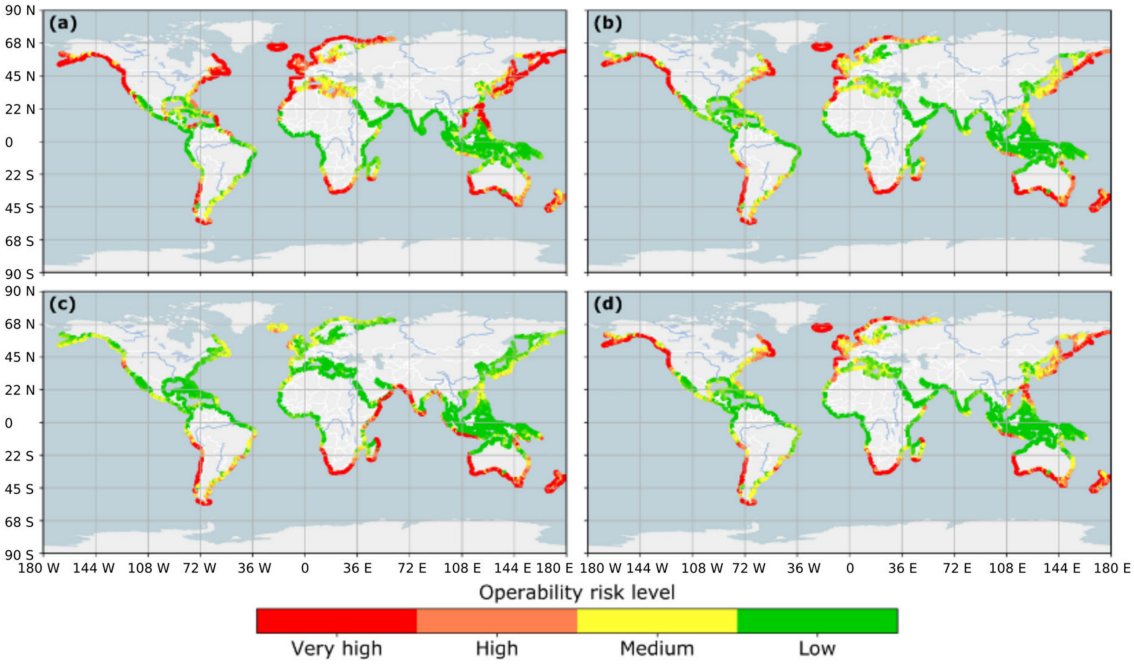


Figure 7. Geographical overview on port operability risk for four separate seasons: (**a**) DJF; (**b**) MAM; (**c**) JJA; (**d**) SON.

The average overall conditional availability, the conditional availability per indicator, and the frequency and duration of exceedance events are analyzed for the separate seasons (see Table 5). For DJF, MAM, JJA, and SON the global average overall conditional availability is 85.0%, 90.4%, 91.3%, and 88.3% respectively. The maximum absolute difference between a season (DJF) and the average over 1979–2018 is 3.9%, which means that sensitivity in terms of seasonality is present, albeit to a small extent.

Table 5. Overview of seasonality effects (DJF/MAM/JJA/SON) on globally averaged overall conditional availability.

Analyzed Time Period	Average Conditional Availability [%]	Conditional Availability per Risk Indicators			Frequency [Events/Season]	Average Duration per Event [hours]
		Wind [%]	Short Waves [%]	IG Waves [%]		
DJF	85.0 (−3.9)	96.4	88.6	88.5	8.9	23.0
MAM	90.4 (+1.5)	98.4	92.2	92.8	6.4	21.0
JJA	91.3 (+2.4)	99.0	92.7	93.7	5.1	21.0
SON	88.3 (−0.6)	97.7	90.7	91.2	7.9	21.8
1979–2018	88.9	97.9	91.1	91.6	28 [1]	24.5

[1] Frequency in terms of events per year.

Short waves are the most critical port operability risk indicator for the analyzed time period 1979–2018, but during DJF, the average conditional availability for IG waves is slightly lower. This is probably due to higher short-wave conditions. The frequency (number of exceedance events per season) distributed over the different seasons shows an

increase in DJF and SON, and the same goes for the average duration of the exceedances. This global seasonality dependency reflects that in our global analysis more locations are present in the northern hemisphere, for which the months SON and DJF correspond to the winter season with harsher wind and wave conditions, than in the southern hemisphere. Note that the sum of the frequency and the average of the duration of the season is not equal to the values for the whole analyzed time period. By splitting the data into seasons and then applying our method season by season, the exceedance events are split at the beginning and end of a season.

3.2.2. Inter-Annual Trends

To assess the sensitivity to changing metocean conditions over the years, the inter-annual trends are analyzed. Inter-annual variations in the global ERA5 database are determined with intervals of one-year and a trendline with an average of the past five years. Instead of looking at the overall average conditional availability over 40 years, the annual average conditional availability is determined, including duration and frequency, and plotted in Figure 8.

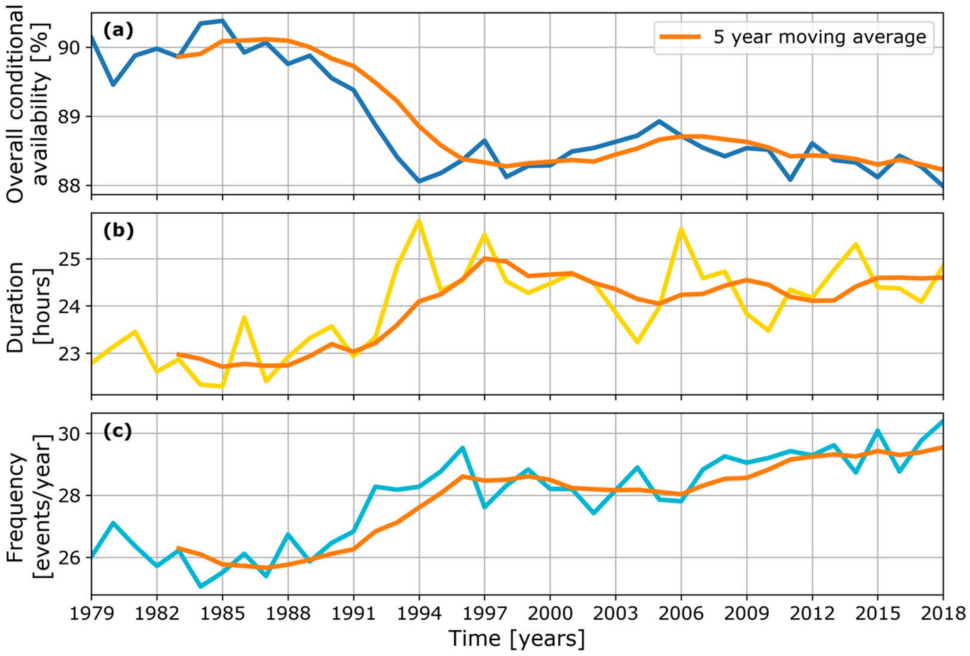


Figure 8. Identifying global trends based on: (**a**) the overall annual average conditional availability; (**b**) duration; (**c**) frequency; from 1979 to 2018. The orange line represents the 5-year moving average.

From Figure 8 it can be concluded that the annual average conditional availability decreases by about 2% over a period of 40 years (Figure 8a). The average annual duration of exceedance events increases by about 2 h (Figure 8b) and the average annual frequency by about five events per year (Figure 8c). What stands out is the sharp decline in overall conditional availability between 1990 and 1995.

To explain the sharp decline and identify the driving forces behind those large global trends in overall conditional availability, the 95th percentile of different metocean parameters (wind speed, short-wave height and IG-wave height) is analyzed over time (see Figure 9). The annual average wind speed increases slightly over a period of 40 years and is relatively insensitive (see Figure 9a). The short-wave height (see Figure 9b) shows a clear increase of about 5%, including a sharp increase between 1990 and 1995 which may explain the sharp decline of overall conditional operability in Figure 8a. The sharp increase in short-wave height can be explained by the use of satellites from 1991 onwards to obtain altimeter wave height data for data assimilation [33]. Both short wave and IG wave drivers

are shown to be more sensitive over time than wind, showing a consistent increase from 1996 in short-wave height and IG-wave height, implicating an increase in port operability risk (i.e., decreasing overall conditional availability) as shown in Figure 8.

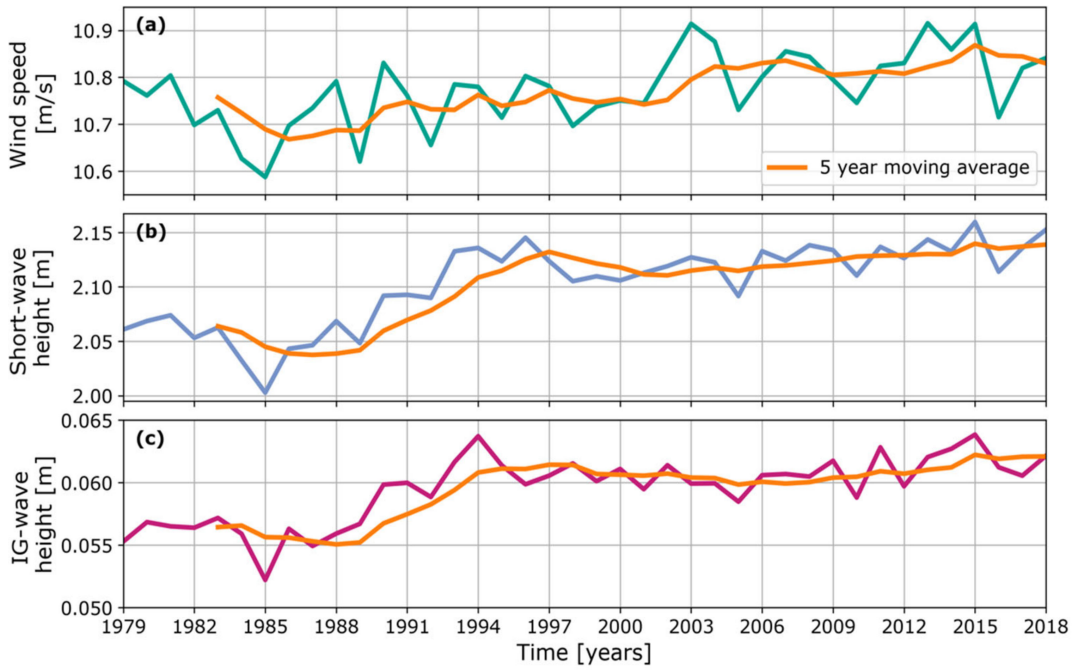


Figure 9. Identifying the driving conditions behind the global trends based on the annual 95th percentiles of the metocean parameters: (**a**) wind speed; (**b**) short-wave height; (**c**) IG-wave height; from 1979 to 2018. The orange line represents the 5-year moving average.

Now the (historic) trend of the overall conditional availability is analyzed in more detail. Instead of looking at the average global trend, the trend for every single location is analyzed. To derive the location specific trend over the past 40 years, the average overall conditional availability is taken for the first 10 years (1979–1988) and the last 10 years (2009–2018) in our dataset to calculate the absolute difference. In this way, the sharp increase in risk due to the inclusion of satellite data can also be circumvented.

The absolute change of the overall conditional availability for each location provides insight into the global temporal patterns of port operability risks, visualized in Figure 10. What stands out is that (port) locations on the southern hemisphere and in particular around the 'Roaring Forties' seem to have a stronger temporal change than (port) locations on the northern hemisphere. The driving conditions are probably higher due to the swell wave climate due to long fetches and the wind speeds that are relatively larger year-round in the southern hemisphere than in the northern hemisphere. The temporal change may be explained by big climate patterns affecting the temperatures in certain parts of the world and having a major influence on the driving conditions [55]. In the southern hemisphere, the temperature differences between ocean and nearby land areas may have been increased due to global warming affecting the flow of air. It is also especially on the western side of the continents, probably due to the strong westerly winds. The southern part of the North Sea is dark blue, indicating a trend of declining port operability risk. This is interesting because this is one of the busiest shipping regions in the world. The reason for an increasing overall conditional availability is probably caused by milder wind and wave conditions. Both observations are substantiated by Takbash and Young [56], who see an increase in either the frequency or intensity of winter storms, particularly in the Southern Ocean, and observe weaker negative trends for the northern hemisphere.

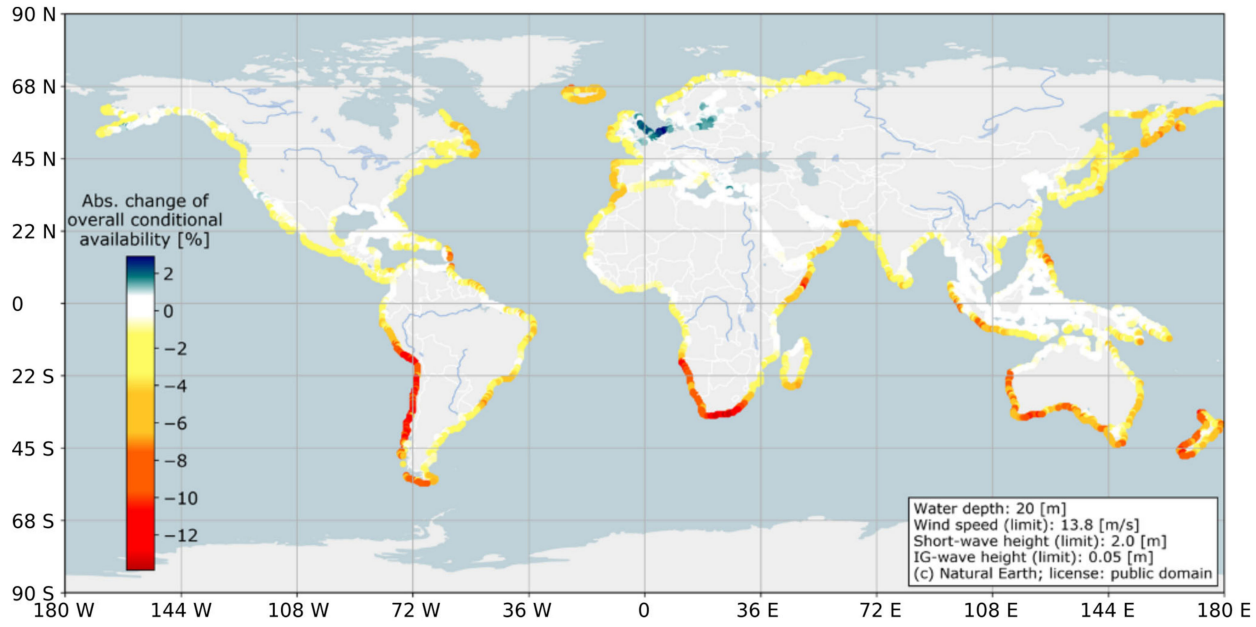


Figure 10. Geographical overview on the absolute change of overall conditional availability between 1979–2018. The dark red dots indicate locations where the risk levels change drastically negatively and the blue dots that change positively (dark blue). Input/thresholds used in the methodology are given in the lower right corner.

4. Discussion

4.1. Validity and Limitations of the Developed Approach

4.1.1. Selected Metocean Indicators

We focus on the environmental conditions that are important for the operability of seaports. Several other studies have also stressed the importance of wind and wave conditions for port operability [18,19,27,57,58]. However, there are more factors that influence the port operability risk, such as the dynamic response of the ships, the port infrastructure and layout (affecting wave breaking, sheltering, diffraction, and reflections), the type of cargo, and the available mooring systems. Therefore, port practitioners should take this wider range of factors into account in their assessments. Nevertheless, wind and wave conditions cannot be controlled directly by the authorities or operators. Therefore, they are a critical element in the trade-off between the degree of protection from external conditions and the operability. With the first-order (viz. pre-intervention) estimates of the operability risks provided in this study, port practitioners can obtain quick insights into the relevance and order of magnitude of wind and wave conditions to assess whether additional measures are required.

Our study accounts for (bound) IG waves by applying a simplified approach. However, in reality, free IG waves are known to be important in the coastal zone. Rawat et al. [59] showed that free IG waves radiating from coastlines along the eastern boundaries of ocean basins are the origin of the largest energy bursts in the infragravity band. IG waves are therefore not limited to a certain area. The calculated IG wave height in this study is probably an underestimation of the IG wave heights in reality. Nevertheless, the bound infragravity wave energy provides a good indication whether these waves are important to consider for port operations at a specific location.

Due to the scale and resolution of this study, the results should be seen as complementary to local scale-studies. Our approach gives a first indication of the expected operability risks and main drivers (preceding detailed studies), which can further be verified in a local scale assessment accounting for the factors that we are now excluding. The benefit of our global-scale assessment is that it allows to intercompare locations and identify large-scale patterns informing the port sector in the explorative stages of port development.

4.1.2. Limitations of Global Datasets

The depth profile is of great importance in the evaluation of the short and IG waves. However, a high-resolution depth profile for all considered locations is not available on a global scale. The accuracy of our conditional availability estimates depends fundamentally on the accuracy of the ERA5 Re-Analysis dataset from ECMWF. We chose grid locations close, but not too close to the coast due to the relatively large resolution of ERA5 which makes it unsuitable to capture small islands and small-size shallow flats/ridges or troughs. The ERA5 significant wave height shows a good agreement with measured buoy data in coastal and deep waters but during tropical cyclones the significant wave height is underestimated [54]. A performance assessment of ERA5 in the Arabian Sea using a wave buoy moored offshore Port of Salalah from early August to late December 2013 with a local depth of 30 m was compared via back-propagation approach to the nearest ERA5 grid point (55 km offshore) [53]. During the monsoon period, the ERA5 significant wave height showed to be less accurate, which shows that under specific conditions the reliability of the data used may be lower.

Due to the limitations of global data in the nearshore, the port operability risk map can only be used as a first-order insights. We found that the ERA5 data differ significantly over a distance of 55 km (between grid points) close to the coast. Hence, locations off the coast with a distance between 0.1–0.8° (respectively 10–100 km) may still be too close. In further research, we suggest using offshore locations with a minimum distance of 0.5° from the coast, because we observe less difference between locations further offshore than locations less than 0.5° offshore. Overall, we believe that ERA5 is a reliable database to provide first-order operability estimates based on metocean conditions on a global scale.

For global information on the nearshore wave characteristics, we used a wave energy balance [35] and assumed an alongshore uniform coast with parallel depth contours and a linear depth profile. This allowed us to gain a global picture on the nearshore wave characteristics within feasible computation times. Applying numerical wave models such as SWAN [12] would have resulted in more reliable nearshore wave information, as these models account for physical processes such as wind growth, white capping, and bed friction. Nevertheless, also for these models we would have to rely on limited information on the bathymetry and the layout and, moreover, they would be much more computationally intensive. As the wave energy balance still accounts for important wave physics, such as shoaling, refraction, and breaking (using a breaker criterion), the method is believed to be sufficiently accurate for this global scale analysis. Nevertheless, for local-scale studies, it is recommended to apply numerical wave models together with local data on the bathymetry and port geometry to calculate the nearshore wave conditions more accurately.

Still, the global spatial and temporal patterns in operability indicators found in our study are consistent with previous studies. Vettor and Soares [32] confirm the energetic wave climate around the capes (as also reflected in Figure 5). Furthermore, [32] also indicated that the wind conditions, which are the main driver for ocean waves, show stronger seasonality in the northern hemisphere than in the southern hemisphere (resembling the patterns in Figure 7). Moreover, the observation that the tropics generally represent milder conditions, hence higher operability, except for the summer monsoons, especially in the Indian Ocean, is consistent with [24,32]. Therefore, the global port operability risk estimates can provide useful first-order (viz. pre-intervention) insights into which regions and which type of operability risks can be expected for ports due to wind and wave conditions.

4.1.3. Selected Operability Thresholds

The chosen operability thresholds for defining the availability in terms of wind, short waves and infragravity waves are based on literature. These are high-level thresholds based on aggregated metocean data, which is a common approach for these types of global assessment [24]. However, in reality, the operability thresholds are determined by the maximum acceptable ship motions, induced by the metocean conditions, for safe and efficient operations [4]. To analyze the uncertainty in the results of our approach,

multiple sensitivity tests are performed by changing the operability thresholds. The results are sensitive for changing operability thresholds, which was also the expectation. We referred to literature values as accessible global information on operability thresholds is lacking. Therefore, the results of this study should be seen as preliminary estimates of port operability risk, but they do illustrate the conditioned thresholding approach and combination of multiple metocean indicators over time.

In this paper, we used fixed operability thresholds and we did not differentiate between the type of cargo and the corresponding operability thresholds (as in [40,45]). The increasing containerization of world trade and the fact that ships want to spend less time berthed in ports is accompanied by stricter operability thresholds. Our model can be re-run with cargo specific operability thresholds to map the operability risks for different cargo types based on the metocean indicators. In the presented results no conclusions are provided yet about the port operability risks for specific cargo types, but by varying the applied thresholds to applicable values, the method is suitable to provide such insights.

4.2. Implications for Existing and Future Port Developments

Our study demonstrates that port operability risk estimates based on global metocean indicators provide realistic first-order insights into port operability risks. This allows port authorities, operators, and designers to quickly scan existing port locations where operability issues can be expected, which locations are potentially suitable for new port developments, and where operability risks change due to changing metocean conditions (e.g., due to climate change), changing water depths (e.g., due to deepening or sea level rise), or changing operability limits (e.g., due to different cargo or ship types).

It is stressed that the spatial and temporal patterns in terms of port operability presented in this paper are subject to change (as already indicated in Figure 10). Climate change is expected to change these patterns even more drastically. Izaguirre et al. [24] performed a global multi-hazard climate change risk assessment for ports, also including indicators like coastal flooding, temperature and precipitation. The study of [24] indicates that low-risk regions in our study, such as the Red Sea and the Mediterranean, can be high risk regions in the future, although this is mainly related to temperature and coastal flooding risks, which are not included in our study. Furthermore, [24] confirms that the high winds around the Roaring Forties, will continue to hamper port operability in this region in the future. The awareness of main drivers, trends in main drivers and possible sensitivities to changing climate can help port authorities, operators, and designers to identify operability risks for existing port locations, intercompare locations to identify large-scale patterns and trends which can be useful to quickly analyze global effects, as well as find suitable (new) port locations where port operability risks are as low as possible. This study therefore provides the opportunity to future-proof both existing and new ports and to respond with the necessary mitigating measures and layout designs to obtain a certain desired operability risk level.

4.3. Opportunities for Future Applications

There is also a trend of more global data becoming available allowing for fusion of these datasets to obtain a more integral view on relevant port indicators. For example, water levels and currents are not included in our operability study. Water level data are relevant for the design of a port, the depth of the approach channel, and the positioning of the fenders in relation to the ship [41,44]. Currents are in most cases relevant for sedimentation and operational dredging costs, leading to operational downtime and expensive maintenance dredging [60]. Because of the case specific characteristics for water levels and currents we did not include these indicators in our study. However, for some locations, water levels and currents are the dominant factors. Numerical models, e.g., the Global Tide and Surge Model (GTSM) from GLOSSIS [61], are available and could be used to include these indicators in our model. The GTSM data are available on the same grid as ERA5 with hourly values. This allows our generic method to apply without adjustments

after defining a common operability threshold for these parameters. Port operability is also sensitive to many other factors, such as climate change, increasing ship traffic, modernized port facilities and changing cargo types. Global scale data on these factors may allow for more integral assessments of port indicators and the effects of (global) developments on these indicators.

5. Conclusions

Ports are crucial nodes in the world's supply chain. Therefore, it is important that port operations can continue as much as possible independent of wave and weather conditions. In this study, we provided insights into the global-scale spatial and temporal patterns in (pre-intervention) port operability risks due to wind and wave conditions based on open-source data. Our method, which was successfully verified for 10 port locations, applies a threshold-based approach to quantify the conditional port availability (i.e., the percentage of time that all wave and wind conditions are below their thresholds) for 4560 coastal locations worldwide. The conditional port availability (P_{total}) is an indicator of (pre-intervention) port operability risk: high availability implies a low risk and, vice versa, low availability implies a high risk. The developed method enables mapping of spatial and temporal port operability risks as well as identifying the driving parameters for these risks on a global scale.

Our results show that the "hotspots" in terms of operability risks ($P_{total} \leq 75\%$) are found along the southern capes, around the 'Roaring Forties' and at exposed locations along the oceans. Locations on and around the equator and around inland seas tend to have an average to low operability risk ($P_{total} > 95\%$). There is a clear difference between winter (DJF) with high operability risk and summer (JJA) with low operability risk, especially in the northern hemisphere. The southern hemisphere shows a high operability risk all year round. This information can be used to identify at which locations (and when) higher/lower risks and/or additional costs for mitigating measures are expected.

For most locations (80.4%), short waves (31.4%), infra-gravity (IG) waves (9.7%), or a combination thereof (39.3%) are the most critical indicators for the expected pre-intervention port operability risk. This implies that mitigating measures should focus on reducing the wave energy and impacts near and inside the port to obtain a sufficient service level. For short wave measures, breakwaters, (changes in) layout orientation, and/or mooring systems are available to mitigate the risks. For IG waves, such mitigating measures are less trivial. The results of our study provide an indication of locations where additional investigations into the importance of short and IG waves are required to further quantify the associated operability risks and identify appropriate mitigating measures.

The temporal trends over the past 40 years show that the annual average conditional availability decreases by about 2%, caused by the slightly increased wind speed, short wave height, and IG wave height. Locations on the southern hemisphere and in particular around the "Roaring Forties" have a stronger temporal change than (port) locations on the northern hemisphere. This implies that operability risks are (slightly) increasing in time and mitigating measures may be required, especially if climate change is also to be accounted for.

The results of our study can help port operators, planners, and financers to identify operability risks for both existing and new port locations at an early stage. This information can be used for the site selection of new port locations, as well as to identify the expected need and costs of mitigating measures for existing port locations. Furthermore, information on the operability drivers can inform which type of mitigating measures may be available and effective. As our results are based on global data, they remain high-level. Therefore, for local applications, the global insights need to be further complemented and verified with more detailed studies, accounting for local aspects such as the bathymetry, the influence of the port layout (wave breaking, sheltering, diffraction, and reflections), and details of ship characteristics, cargo, and mooring systems.

Author Contributions: M.W. developed the method of the study, developed all code, analyzed the results, created all figures, and prepared the original manuscript—as MSc student at Delft University of Technology and graduate intern at Deltares; W.d.B. conceived the idea and methodology for the study, supervised the project, and assisted in writing, editing, and reviewing the manuscript; A.v.d.H. contributed to the analysis of the wave data, supervision, reviewing, and editing of the manuscript; A.R. contributed to the IG wave analysis, supervision, interpretation of results, as well as reviewing and editing of the manuscript; M.v.K. coordinated the supervision of the project, contributed to the interpretation of results, and assisted in editing and reviewing the manuscript. All authors have read and agreed to the published version of the manuscript.

Funding: This work was supported by the Deltares strategic research program "Future-proof Coastal Infrastructure and Offshore Renewable Energy" (2020) and "Infrastructure Systems" (2021).

Institutional Review Board Statement: Not applicable.

Informed Consent Statement: Not applicable.

Data Availability Statement: Not applicable.

Acknowledgments: We would like to thank the European Centre for Medium-Range Weather Forecasts (ECMWF) for making the ERA5 data open-source available.

Conflicts of Interest: The authors declare no conflict of interest.

Appendix A

The nearshore wave climate is used as spectral input for evaluating the IG waves by Herbers et al. [36], who stated that second-order non-linear theory from Hasselmann [37] accurately predicts locally forced infragravity motions. Non-linear interactions of two surface gravity waves (with slightly different frequencies $f_1 = f$ and $f_2 = f + \Delta f$) excite a forced secondary wave with the difference-frequency Δf. The energy of the secondary forces surface elevation $E_{forced}(\Delta f)$ for one pair of interacting primary waves is computed with the following expression described by Van Dongeren et al. [38]:

$$E_{forced}(\Delta f) = 2 \int_{\Delta f}^{\infty} \int_{0}^{2\pi} \int_{0}^{2\pi} \mathrm{D}^2(f + \Delta f, -f, \Delta\theta + \pi)\, E(f + \Delta f, \theta_1)\, E(f, \theta_2)\, d\theta_2\, d\theta_1\, df,$$

$E_{forced}(\Delta f)$ is the bound long wave energy (m^2/Hz). $E(f, \theta)$ is the 2D frequency-directional spectrum of primary (sea and swell) waves (m^2/Hz). Subscripts 1 and 2 refer to the two interacting primary waves. $\mathrm{D}(f + \Delta f, -f, \Delta\theta + \pi)$ is the difference-interaction coefficient with a difference in propagation directions of the interacting pair of primary wave components with directions: $\Delta\theta = |\theta_1 - \theta_2|$. This difference-interaction coefficient for the surface elevation energy is defined as:

$$\begin{aligned}\mathrm{D}(-f_1, f_2, \Delta\theta + \pi) \equiv{}& \frac{\mathrm{g k_1 k_2} \cos(\Delta\theta + \pi)}{8\pi^2 f_1 f_2} \frac{\cosh(\mathrm{k_3 h})}{\cosh(\mathrm{k_1 h}) \cosh(\mathrm{k_2 h})} - \frac{\mathrm{g}(-f_1 + f_2)}{\left[\mathrm{g k_3} \tanh(\mathrm{k_3 h}) - (2\pi)^2 (-f_1 + f_2)^2\right] f_1 f_2} \times \\ & \left\{ (-f_1 + f_2) \left[\frac{(2\pi)^4 (f_1 f_2)^2}{\mathrm{g}^2} - \mathrm{k_1 k_2} \cos(\Delta\theta + \pi) \right] - \frac{1}{2} \left[\frac{-f_1 \mathrm{k_2}^2}{\cosh^2(\mathrm{k_2 h})} + \frac{f_2 \mathrm{k_1}^2}{\cosh^2(\mathrm{k_1 h})} \right] \right\},\end{aligned}$$

In this equation, the wave number, $\mathrm{k_3}$ of the bound IG wave is equal to the difference in wave number of the two short waves:

$$\mathrm{k_3} \equiv \left| \vec{\mathrm{k_1}} - \vec{\mathrm{k_2}} \right| = \sqrt{\mathrm{k_1}^2 + \mathrm{k_2}^2 - 2\mathrm{k_1 k_2} \cos(\Delta\theta)}$$

From the estimated bound waves, the representative wave height $\mathrm{H_{m0,Low}}$ and mean wave period $\mathrm{T_{m01,Low}}$ are determined based on the zeroth-order and first-order moments of the spectral density.

References

1. UNCTAD. Review of Maritime Transport 2018. United Nations Publication. 2018. Available online: https://stats.unctad.org/handbook/MaritimeTransport/WorldSeaborneTrade.html (accessed on 6 November 2019).
2. Mudronja, G.; Jugović, A.; Škalamera-Alilović, D. Seaports and economic growth: Panel data analysis of EU port regions. *J. Mar. Sci. Eng.* **2020**, *8*, 1017. [CrossRef]
3. UNCTAD. *Port Industry Survey on Climate Change Impacts and Adaptation*; UNCTAD: Geneva, Switzerland, 2018.
4. Molina-Sanchez, R.; Campos, Á.; De Alfonso, M.; Santos, F.J.D.L.; Rodríguez-Rubio, P.; Pérez-Rubio, S.; Camarero-Orive, A.; Álvarez-Fanjul, E. Assessing Operability on Berthed Ships. Common Approaches, Present and Future Lines. *J. Mar. Sci. Eng.* **2020**, *8*, 255. [CrossRef]
5. Okihiro, M.; Guza, R.T.; Seymour, R.J. Excitation of seiche observed in a small harbor. *J. Geophys. Res. Space Phys.* **1993**, *98*, 18201. [CrossRef]
6. Bowers, E.C. Harbour resonance due to set-down beneath wave groups. *J. Fluid Mech.* **1977**, *79*, 71–92. [CrossRef]
7. Cuomo, G.; Guza, R.T. Infragravity Seiches in a Small Harbor. *J. Waterw. Port Coast. Ocean Eng.* **2017**, *143*, 04017032. [CrossRef]
8. Bellotti, G. Transient response of harbours to long waves under resonance conditions. *Coast. Eng.* **2007**, *54*, 680–693. [CrossRef]
9. Herbers, T.H.C.; Elgar, S.; Guza, R.T. Generation and propagation of infragravity waves. *J. Geophys. Res. Space Phys.* **1995**, *100*, 24863–24872. [CrossRef]
10. López, M.; Iglesias, G. Long wave effects on a vessel at berth. *Appl. Ocean Res.* **2014**, *47*, 63–72. [CrossRef]
11. Sakakibara, S.; Kubo, M. Characteristics of low-frequency motions of ships moored inside ports and harbors on the basis of field observations. *Mar. Struct.* **2008**, *21*, 196–223. [CrossRef]
12. Booij, N.; Holthuijsen, L.; Ris, R. 'SWAN' wave model for shallow water. In Proceedings of the Coastal Engineering Conference, Orlando, FL, USA, 2–6 September 1996; Volume 1, pp. 668–676. [CrossRef]
13. Massey, T.C.; Anderson, M.E.; Smith, J.M.; Gomez, J.; Jones, R. *STWAVE: Steady-State Spectral Wave Model User's Manual for STWAVE, Version 6.0*; Technical Report; U.S. Army Corps of Engineers, Engineer Research and Development Center, Coastal and Hydraulics Laboratory: Vicksburg, MI, USA, 2011.
14. DHI. *MIKE 21 SW-Spectral Wave Model Short Description*; DHI: Horsholm, Denmark, 2017.
15. Deltares. PHAROS-User & Technical Manual. 2016. Available online: https://www.deltares.nl/en/software/pharos/ (accessed on 1 June 2020).
16. Deltares. TRITON-User & Technical Manual. 2008. Available online: https://www.oss.deltares.nl (accessed on 1 June 2020).
17. Zijlema, M.; Stelling, G.; Smit, P. SWASH: An operational public domain code for simulating wave fields and rapidly varied flows in coastal waters. *Coast. Eng.* **2011**, *58*, 992–1012. [CrossRef]
18. Rusu, E.; Soares, C.G. Wave modelling at the entrance of ports. *Ocean Eng.* **2011**, *38*, 2089–2109. [CrossRef]
19. Rusu, L.; Soares, C.G. Evaluation of a high-resolution wave forecasting system for the approaches to ports. *Ocean Eng.* **2013**, *58*, 224–238. [CrossRef]
20. Diaz-Hernandez, G.; Mendez, F.J.; Losada, I.J.; Camus, P.; Medina, R. A nearshore long-term infragravity wave analysis for open harbours. *Coast. Eng.* **2015**, *97*, 78–90. [CrossRef]
21. Van Der Hout, A.J.; De Jong, M.P.C.; Moerman, E.; Timerman, G.J.; Ribeiro, E.O. Determination of infragravity wave conditions at a nearshore location with a non-uniform coastline-Case study of Baía de Todos os Santos, Brazil. In Proceedings of the ASME 2012 31st International Conference on Ocean, Offshore and Arctic Engineering, Rio de Janeiro, Brazil, 1–6 July 2012; Volume 5, pp. 249–257. [CrossRef]
22. Campos, Á.; García-Valdecasas, J.M.; Molina, R.; Castillo, C.; Álvarez-Fanjul, E.; Staneva, J. Addressing long-term operational risk management in port docks under climate change scenarios-A Spanish case study. *Water* **2019**, *11*, 2153. [CrossRef]
23. Camus, P.; Tomás, A.; Díaz-Hernández, G.; Rodríguez, B.; Izaguirre, C.; Losada, I. Probabilistic assessment of port operation downtimes under climate change. *Coast. Eng.* **2019**, *147*, 12–24. [CrossRef]
24. Izaguirre, C.; Losada, I.J.; Camus, P.; Vigh, J.L.; Stenek, V. Climate change risk to global port operations. *Nat. Clim. Chang.* **2021**, *11*, 14–20. [CrossRef]
25. Sierra, J.P.; Casanovas, I.; Mösso, C.; Mestres, M.; Sánchez-Arcilla, A. Vulnerability of Catalan (NW Mediterranean) ports to wave overtopping due to different scenarios of sea level rise. *Reg. Environ. Chang.* **2016**, *16*, 1457–1468. [CrossRef]
26. Camus, P.; Losada, I.J.; Izaguirre, C.; Espejo, A.; Menéndez, M.; Pérez, J. Statistical wave climate projections for coastal impact assessments. *Earth's Future* **2017**, *5*, 918–933. [CrossRef]
27. Sierra, J.P.; Casas-Prat, M.; Virgili, M.; Mösso, C.; Sanchezarcilla, A. Impacts on wave-driven harbour agitation due to climate change in Catalan ports. *Nat. Hazards Earth Syst. Sci.* **2015**, *15*, 1695–1709. [CrossRef]
28. Gracia, V.; Sierra, J.P.; Gómez, M.; Pedrol, M.; Sampé, S.; García-León, M.; Gironella, X. Assessing the impact of sea level rise on port operability using LiDAR-derived digital elevation models. *Remote Sens. Environ.* **2019**, *232*, 111318. [CrossRef]
29. Sierra, J.; Genius, A.; Lionello, P.; Mestres, M.; Mösso, C.; Marzo, L. Modelling the impact of climate change on harbour operability: The Barcelona port case study. *Ocean Eng.* **2017**, *141*, 64–78. [CrossRef]
30. Dee, D.P.; Uppala, S.M.; Simmons, A.J.; Berrisford, P.; Poli, P.; Kobayashi, S.; Andrae, U.; Balmaseda, M.A.; Balsamo, G.; Bauer, P.; et al. The ERA-Interim reanalysis: Configuration and performance of the data assimilation system. *Q. J. R. Meteorol. Soc.* **2011**, *137*, 553–597. [CrossRef]

31. De Boer, W.; Mao, Y.; Hagenaars, G.; De Vries, S.; Slinger, J.; Vellinga, T. Mapping the Sandy Beach Evolution Around Seaports at the Scale of the African Continent. *J. Mar. Sci. Eng.* **2019**, *7*, 151. [CrossRef]
32. Vettor, R.; Soares, C.G. A global view on bimodal wave spectra and crossing seas from ERA-interim. *Ocean Eng.* **2020**, *210*, 107439. [CrossRef]
33. ECMWF. Copernicus Climate Change Service (C3S) (2017): ERA5: Fifth Generation of ECMWF Atmospheric Reanalyses of the Global Climate. Copernicus Climate Change Service Climate Data Store (CDS). 2019. Available online: https://cds.climate.copernicus.eu/cdsapp#!/home (accessed on 1 November 2019).
34. Natural Earth Data. Natural Earth. Free Vector and Raster Map Data. 2020. Available online: https://www.naturalearthdata.com/ (accessed on 8 April 2020).
35. Battjes, J.A.; Stive, M.J.F. Calibration and verification of a dissipation model for random breaking waves. *J. Geophys. Res. Space Phys.* **1985**, *90*, 9159–9167. [CrossRef]
36. Herbers, T.H.C.; Elgar, S.; Guza, R.T. Infragravity-frequency (0.005-0.05 Hz) motions on the shelf. Part I: Forced waves. *J. Phys. Oceanogr. J. Phys. Oceanogr.* **1994**, *24*, 917–927. [CrossRef]
37. Hasselmann, K. On the non-linear energy transfer in a gravity-wave spectrum: Part 3. Evaluation of the energy flux and swell-sea interaction for a Neumann spectrum. *J. Fluid Mech.* **1963**, *15*, 385–398. [CrossRef]
38. Van Dongeren, A.; Reniers, A.; Battjes, J.; Svendsen, I. Numerical modeling of infragravity wave response during DELILAH. *J. Geophys. Res. Space Phys.* **2003**, *108*, C9. [CrossRef]
39. PIANC. *Report No. 24 Criteria for Movements of Moored Ships in Harbours—A Practical Guide*; PIANC: Brussels, Belgium, 1995.
40. PIANC. *Report No. 115 Criteria for the (Un)loading of Container Vessels*; PIANC: Brussels, Belgium, 2012.
41. PIANC. *Report No. 121 Harbour Approach Channels Design Guidelines*; PIANC: Brussels, Belgium, 2014.
42. Van den Bos, W. *Wind Influence on Container Handling, Equipment and Stacking*; Port Technology International: London, UK, 2011; Volume 29, pp. 89–95. Available online: https://www.porttechnology.org/technical-papers/wind_influence_on_container_handling_equipment_and_stacking/ (accessed on 1 December 2019).
43. Mol, A.; Ligteringen, H.; Waanders, A.J. Motions of moored vessels, a statistical approach. In Proceedings of the Australasian Port, Harbour & Offshore Engineering Conference, Sydney, Australia, 29 September–2 October 1986; pp. 141–145.
44. Thoresen, C.A. *Port Designer's Handbook*; ICE Publishing: London, UK, 2018. [CrossRef]
45. Ligteringen, H.; Velsink, H. *Ports and Terminals*, 2nd ed.; Delft Academic Press: Delft, The Netherlands, 2017.
46. Mesa, C.; Wesley, M. Hurricane Marie and the Port of Long Beach, California, USA. In Proceedings of the 36th Conference on Coastal Engineering, Baltimore, MD, USA, 30 July–3 August 2018; Volume 36, p. 2008. [CrossRef]
47. Van Der Molen, W.; Monárdez, P.; Van Dongeren, A. Numerical simulation of long-period waves and ship motions in Tomakomai Port, Japan. *Coast. Eng. J.* **2006**, *48*, 59–79. [CrossRef]
48. Carr, C.M.; Yavary, M.; Yavary, M. Wave agitation studies for port expansion-Salalah, Oman. In Proceedings of the Ports Conference 2004: Port Development in the Changing World, Houston, TX, USA, 23–26 May 2004; pp. 71–80. [CrossRef]
49. Van der Molen, W.; Moes, H. General characteristics of South African ports and the safe mooring of ships. In Proceedings of the 28th Annual Southern African Transport Conference, Pretoria, South Africa, 6–9 July 2009; pp. 308–314.
50. Duplex, P. Technical Symposium Long Period Wave Mitigation–Geraldton Harbour. In Proceedings of the Technical Symposium of Long Period Wave Mitigation–Geraldton Harbour; Mid West Ports Authority, Geraldton, Australia, 27–29 May 2014; p. 149.
51. Van Der Molen, W.; Scott, D.; Taylor, D.; Elliott, T. Improvement of mooring configurations in Geraldton harbour. *J. Mar. Sci. Eng.* **2015**, *4*, 3. [CrossRef]
52. Google. Google Maps Location for Port in Doraleh. Google Maps. Available online: https://www.google.com/maps/place/Port+de+Doraleh/@11.5872327,43.0711369,7945m/data=!3m1!1e3!4m5!3m4!1s0x162301536ddfe9e1:0x6045322c29a2db5e!8m2!3d11.5938528!4d43.1056507 (accessed on 26 November 2019).
53. Bruno, M.F.; Molfetta, M.G.; Totaro, V.; Mossa, M. Performance Assessment of ERA5 Wave Data in a Swell Dominated Region. *J. Mar. Sci. Eng.* **2020**, *8*, 214. [CrossRef]
54. Naseef, T.M.; Kumar, V.S. Climatology and trends of the Indian Ocean surface waves based on 39-year long ERA5 reanalysis data. *Int. J. Climatol.* **2020**, *40*, 979–1006. [CrossRef]
55. Zeng, Z.; Ziegler, A.D.; Searchinger, T.; Yang, L.; Chen, A.; Ju, K.; Piao, S.; Li, L.Z.X.; Ciais, P.; Chen, D.; et al. A reversal in global terrestrial stilling and its implications for wind energy production. *Nat. Clim. Chang.* **2019**, *9*, 979–985. [CrossRef]
56. Takbash, A.; Young, I.R. Long-term and seasonal trends in global wave height extremes derived from era-5 reanalysis data. *J. Mar. Sci. Eng.* **2020**, *8*, 1015. [CrossRef]
57. Hattha, W.; Hiraishi, T. Berth Operability and Port Downtime Due to MetOcean in Eastern Thailand. In Proceedings of the The 27th International Ocean and Polar Engineering Conference, International Society of Offshore and Polar Engineers, San Francisco, CA, USA, 25–30 June 2017; p. 8.
58. Sánchez-Arcilla, A.; Sierra, J.P.; Brown, S.; Casas-Prat, M.; Nicholls, R.J.; Lionello, P.; Conte, D. A review of potential physical impacts on harbours in the Mediterranean Sea under climate change. *Reg. Environ. Chang.* **2016**, *16*, 2471–2484. [CrossRef]
59. Rawat, A.; Ardhuin, F.; Ballu, V.; Crawford, W.; Corela, C.; Aucan, J. Infragravity waves across the oceans. *Geophys. Res. Lett.* **2014**, *41*, 7957–7963. [CrossRef]

60. Winterwerp, J.C. Reducing Harbor Siltation. I: Methodology. *J. Waterw. Port Coast. Ocean Eng.* **2005**, *131*, 258–266. [CrossRef]
61. Verlaan, M.; de Kleermaeker, S.; Buckman, L. GLOSSIS: Global Storm Surge Forecasting and Information System. In Proceedings of the Australasian Coasts & Ports Conference 2015: 22nd Australasian Coastal and Ocean Engineering Conference and the 15th Australasian Port and Harbour Conference, Engineers Australia and IPENZ, Auckland, New Zealand, 15–18 September 2015; p. 229.